Directional Antineutrino Detection

Directional Antineutrino Detection

Benjamin R. Safdi[1,*] and Burkhant Suerfu[2,†]
[1]Center for Theoretical Physics, Massachusetts Institute of Technology, Cambridge, Massachusetts 02139, USA
[2]Department of Physics, Princeton University, Princeton, New Jersey 08544, USA
(Received 4 November 2014; revised manuscript received 24 December 2014; published 20 February 2015)

We propose the first event-by-event directional antineutrino detector using inverse beta decay (IBD) interactions on hydrogen, with potential applications including monitoring for nuclear nonproliferation, spatially mapping geoneutrinos, characterizing the diffuse supernova neutrino background and searching for new physics in the neutrino sector. The detector consists of adjacent and separated target and capture scintillator planes. IBD events take place in the target layers, which are thin enough to allow the neutrons to escape without scattering elastically. The neutrons are detected in the thicker boron-loaded capture layers. The location of the IBD event and the momentum of the positron are determined by tracking the positron's trajectory through the detector. Our design is a straightforward modification of existing antineutrino detectors; a prototype could be built with existing technology.

DOI: 10.1103/PhysRevLett.114.071802 PACS numbers: 13.15.+g, 28.41.-i, 95.55.Vj, 95.85.Ry

Introduction.—We present a realistic proposal for directional antineutrino detection through a design we call SANTA (segmented antineutrino tomography apparatus). Such a detector may have applications to reactor antineutrino monitoring for nuclear nonproliferation (see, for example, Refs. [1–5]). Moreover, the directionality significantly cuts down on background compared to nondirectional detectors. The reduced-background properties of directional detectors make them ideal detectors for short baseline neutrino experiments searching for new physics in the neutrino sector, such as IsoDAR or DAEdALUS [6,7].

A large-volume SANTA with hundreds of tons of target mass would be capable of spatially mapping geoneutrinos [8] and, thus, constructing a map of radioactive material inside Earth. Geoneutrinos have been detected at the KamLAND [9] and Borexino experiments [10], but their measurements lack directionality. Other applications of such a detector to fundamental physics include searching for solar antineutrinos that could indicate neutrino electromagnetic interactions [11,12] and characterizing the predicted diffuse supernova neutrino background [13–15] (see Ref. [16] for a recent review).

Low-energy antineutrinos with energies ∼2–10 MeV are typically detected by inverse beta decay (IBD). The antineutrino scatters inelastically with a proton into a neutron and a positron. The positron quickly loses energy and annihilates with an electron. The neutron diffuses for a longer time before it reaches thermal speeds and is captured.

Current detectors cannot determine the antineutrino's direction on an event-by-event basis because of neutron diffusion. The neutron recoils in approximately the direction of the antineutrino's velocity. However, by the time it is captured, the neutron has little preference to end up in the direction it was originally traveling. Still, some detectors have been able to use statistical methods to extract directional information about the distribution of antineutrinos, including Gosgen [17], Bugey [18], Palo Verde [19,20], and CHOOZ [21]. For example, with ∼2500 total IBD events, the CHOOZ experiment was able to determine the direction of the nuclear power plant where the antineutrinos were produced to within ∼18° at 68% C.L. [21]. The CHOOZ experiment used a 0.09% Gd-loaded liquid scintillator target to minimize the neutron diffusion length. Recently, Ref. [22] studied the advantages of using ^{6}Li-loaded scintillators to increase position resolution and directional sensitivity; they concluded that small improvements in the angular resolution compared to CHOOZ may be possible in the future. The mini Time Cube project [23] plans to use boron-loaded plastic scintillators to improve their directional sensitivity.

Detector concept.—We present a simple detector concept that circumvents the neutron diffusion limitation of previous detectors, which we refer to as monolithic detectors. The idea is to make the target, where IBD events occur, a thin-enough sheet of scintillator so that most neutrons escape without scattering elastically, therefore, preserving the directional information. The neutrons then travel through free space to adjacent capture layers, where they diffuse and are captured (see Fig. 1). The IBD location and the neutron-capture location can be used to deduce the direction of the neutron's momentum $\mathbf{p_n}$. In this Letter, we take the region between layers to be vacuum for simplicity. However, this region may be any low-density medium, such as air, so long as the probability of neutron elastic scattering is small. Charged-particle tracking may also be introduced between layers.

The IBD event location is determined from the positron, which deposits energy within the target layer through ionization, Bhabha scattering, and bremsstrahlung. The positrons may either annihilate within the target layer or

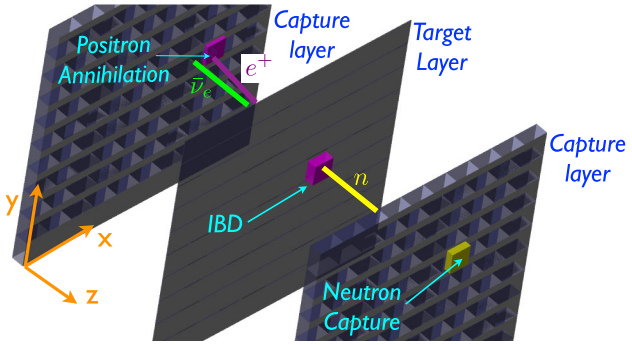

FIG. 1 (color online). The detector consists of alternating layers of plastic scintillator, with the capture layers loaded with boron. IBD events take place in the thin target layers, and the positron subsequently deposits energy (purple boxes) within the target layer and travels to the adjacent thick capture layer, where it annihilates. The neutron propagates freely to the capture layer, where it diffuses and is captured on ^{10}B, depositing energy (yellow box), with a delayed coincidence from the positron annihilation.

escape, traverse between layers, and then lose energy and annihilate in one of the capture layers. The annihilation results in two back-to-back ~0.5 MeV γ's. Within a few nanoseconds of the IBD event, there may be multiple coincident signals from the positron alone. The positron's energy E_{e^+} is measured from the total energy deposited in the detector in this short time. When the positron escapes the target layer, the direction of the positron's momentum $\mathbf{p}_{\mathbf{e}^+}$ may be reconstructed from the spatial and temporal distribution of deposited energy. Charged-particle tracking between layers may also be used to reconstruct $\mathbf{p}_{\mathbf{e}^+}$. It may also be possible to determine $\mathbf{p}_{\mathbf{e}^+}$ within the target layer itself by drifting the secondary ions produced by the positron towards the target-layer sides and measuring the distribution of arrival times and locations (see, for example, Ref. [24]). In the remainder of this Letter, we use Monte Carlo simulations in GEANT4 [25] to demonstrate the directional capability for a specific SANTA configuration.

Detector simulations.—We take the target and capture layers to be plastic scintillators, with the capture layers loaded with 5% natural B by weight, which is commercially available [26]. The ^{10}B is introduced for its high neutron-capture cross section. Moreover, neutron capture on ^{10}B results in an α, γ, and ^{7}Li, with a Q value ~2.78 MeV. The majority of this energy is deposited within a very short distance in the scintillator, which helps identify the neutron capture.

In practice, each layer may consist of stacks of long thin scintillator bars, similar to the PANDA antineutrino experiment [27], the PROSPECT experiment [28], and the DANSSino experiment [29]. Position resolution along the directions of the scintillator bars may be achieved using timing and by comparing the luminosity at the two ends. The finite position resolution in these layers is not expected to be a significant source of error on the reconstructed direction of the antineutrinos, so long as the position resolution is sufficiently smaller than the separation between layers. The Palo Verde experiment [19] used ~9 m long cells with 12×25 cm^2 cross sections of Gd-loaded liquid scintillator. They achieved ~20 cm position resolution on the neutron-capture locations in the longitudinal direction along the cells using the timing difference between the PMTs at the end points of the cells. Better position resolution ~10 (5) cm may be achievable using B- (Li)-loaded scintillators (see, for example, Ref. [22]). We do not model the position resolution within the scintillator sheets in the following simulations, as this depends heavily on the specific experimental configuration. However, in the Supplemental Material [30], we show that realistic position resolutions do not significantly affect the results.

The target layer should be thin enough for most neutrons to escape without elastically scattering off hydrogen or carbon; this corresponds to a target-layer thickness ~1 cm in our material. We illustrate target-layer thicknesses of 0.5, 1, and 2 cm. Most neutrons are captured on ^{10}B within a few centimeters in the boron-loaded plastic scintillator. For definiteness, we take the capture layers to be 6 cm thick. With this thickness, only ~5% of 50 keV neutrons incident normal to the capture layer pass through the layer without capture (neutrons recoiling from reactor-energy antineutrinos have kinetic energies ~1–100 keV). We take the layers to be separated by 1 m, as this is much longer than the thicknesses of each individual layer. Better angular resolution may be achieved by using a longer separation.

The reconstruction of $\mathbf{p}_{\mathbf{e}^+}$ is straightforward once the positron has left the target layer. However, hard scattering within the target layer may deflect the positron before it leaves that layer. Our ability to account for hard scattering within the target layer is sensitive to the specific detector design and energy thresholds. To keep our analysis general, we reconstruct the antineutrino's momentum in two ways. First, we use the neutron's direction alone and equate the unit vectors $\hat{\mathbf{p}}_\nu \approx \hat{\mathbf{p}}_\mathbf{n}$, where $\hat{\mathbf{p}}_\mathbf{n}$ points in the direction of the neutron's reconstructed momentum. Second, we assume that we may exactly reconstruct $\mathbf{p}_\mathbf{e}^+$, and we then use both $\hat{\mathbf{p}}_\mathbf{n}$ and $\mathbf{p}_{\mathbf{e}^+}$ in reconstructing $\hat{\mathbf{p}}_\nu$. See the Supplemental Material [30] for more details on reconstructing $\hat{\mathbf{p}}_\nu$.

A key method for improving the angular resolution is timing. A typical neutron is captured within a few microseconds in the boron-loaded plastic scintillator. However, events where the neutron bounces multiple times between detector layers will be delayed, because as the neutron slows down, it takes time to cross the 1 m gap between layers. Lower timing cuts result in better angular resolution at the cost of a reduced rate. A timing cut between the positron annihilation and neutron capture also helps discriminate from other random-coincidence backgrounds.

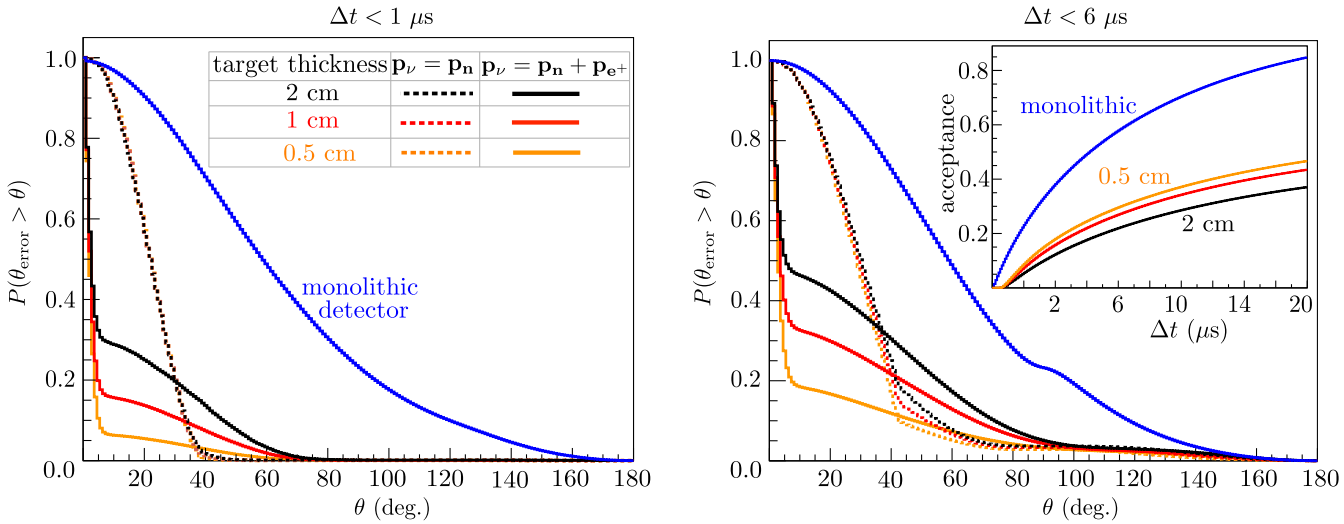

FIG. 2 (color online). We calculate $P(\theta_{\rm error} > \theta)$ for 4 MeV antineutrinos incident normal to the target plane for 0.5, 1, and 2 cm thick target layers, with $\theta_{\rm error}$ the angular error in the reconstruction of $\hat{\mathbf{p}}_\nu$: $\cos\theta_{\rm error} = \hat{\mathbf{p}}_\nu \cdot \hat{\mathbf{p}}_\nu^{\rm rec}$. The antineutrino momentum is reconstructed using two methods. The first method only uses the neutron's reconstructed momentum, $\hat{\mathbf{p}}_\nu^{\rm rec} = \hat{\mathbf{p}}_{\mathbf{n}}$, while the second method uses the reconstructed neutron momentum and the positron momentum, which we assume is reconstructed exactly: $\mathbf{p}_\nu^{\rm rec} = \mathbf{p_n} + \mathbf{p}_{e^+}$. A key tool for improving the angular resolution is timing. The left panel imposes a < 1 μs timing cut between the positron annihilation and the neutron capture, while the right panel uses a < 6 μs timing cut. The stricter timing cuts, however, result in a reduced fraction of events that are accepted by the analysis, as shown in the inset plot on the right panel. For reference, we also show the angular resolution and acceptance rate for a boron-loaded monolithic detector assuming perfect reconstruction of the neutron-capture location and the IBD event location.

Similarly, we require a minimum time delay between the positron event and the neutron capture equal to the amount of time required for the neutron to travel between layers. This time delay depends on the reconstructed neutron momentum, but it is typically ~0.5 μs for reactor-energy antineutrinos.

Another method for discriminating against events where the neutron has scattered significantly before capture is to require $\cos\theta_{en} = \hat{\mathbf{p}}_{e^+} \cdot \hat{\mathbf{p}}_{\mathbf{n}}$ to be less than some minimum value, which we take to be zero in our analysis for definiteness. This cut is more effective at antineutrino energies well above threshold; in the limit $E_{e^+} \gg 1.8$ MeV, the fraction of events with $\cos\theta_{en} > 0$ shrinks to zero. We only perform this cut when reconstructing $\hat{\mathbf{p}}_\nu$ from both $\hat{\mathbf{p}}_{\mathbf{n}}$ and $\mathbf{p}_{e^+}$. See the Supplemental Material [30] for details on the scattering kinematics and analysis.

As an illustration, we perform Monte Carlo simulations for 4 MeV antineutrinos traveling in the direction $\hat{\mathbf{p}}_\nu = \hat{\mathbf{z}}$ (normal to the planes), in the notation of Fig. 1. We generate 10^7 IBD events in the target layer, for each target-layer thickness. We define $\mathbf{p}_\nu^{\rm rec}$ to be the reconstructed neutrino momentum vector and the angular error $\theta_{\rm error}$ of the reconstruction by $\cos\theta_{\rm error} = \hat{\mathbf{p}}_\nu \cdot \hat{\mathbf{p}}_\nu^{\rm rec}$.

In Fig. 2, we show the Monte Carlo determined cumulative probability $P(\theta_{\rm error} > \theta)$ that the angular error is greater than a value θ. We reconstruct $\mathbf{p}_\nu^{\rm rec}$ using the neutron's direction alone (dotted curves) and also by including the exact positron momentum (solid curves). We illustrate the effect of a timing cut $\Delta t < 1$ μs (left panel) and $\Delta t < 6$ μs (right panel). The shorter timing cut results in better angular reconstruction, but fewer events are accepted. The inset plot on the right panel shows the fraction of events accepted as a function of the timing cut.

The positrons are less likely to escape the target layer as the target-layer thickness is increased. For a 0.5 (1) (2) cm target, we find that ~45% (30%) (25%) of the positrons escape the target layer.

The neutron-only reconstructions have similar errors across all target-layer thicknesses; these analyses are limited by the fact that we are neglecting the positron's momentum in reconstructing $\mathbf{p}_\nu$. When we include the positron momenta in the reconstruction, the difference between target-layer thicknesses becomes clearer. In Fig. 2, it may be seen that thinner targets result in better angular resolution when including the positron's momentum in the analysis. For comparison, we also show the cumulative probability for a monolithic detector consisting of the same boron-loaded plastic scintillator that is in the capture layers of the SANTA simulations. In the monolithic simulations, we approximate $\hat{\mathbf{p}}_\nu \approx \hat{\mathbf{p}}_{\mathbf{n}}$ using the exact neutron-capture and IBD event locations. All of our SANTA target-layer thicknesses and $\hat{\mathbf{p}}_\nu$ reconstruction algorithms outperform the monolithic detector. See the Supplemental Material [30] for examples with other antineutrino energies and incident angles.

Discussion.—We have presented a novel design for a directional antineutrino detector that utilizes existing technology, and we have demonstrated its capability through Monte Carlo simulations. The detector works by segmenting

the volume into alternating target and capture layers. The target layers are made thin enough for neutrons to escape with minimal elastic scattering. It is important to note, however, that nondirectional IBD events may also be observed fully within the capture layers, making the detector dual purpose. We have not attempted to optimize the parameters of the detector. There are a number of ways in which our example detector could be improved. The angular resolution increases with increasing distance between layers and decreasing target-layer thickness.

Our design has a variety of potential applications; for example, a small-scale detector with ~1 ton of target scintillator could be used for near-field reactor monitoring [4,5]. Such a detector may consist of a 1 cm thick $\sim 10 \times 10$ m^2 target layer with adjacent equal-area capture layers. The fact that there is empty space between detector layers does present a challenge for the scalability of the detector; a large-mass detector will necessarily take up a lot of physical space. For example, if a kiloton SANTA for geoneutrino detection [9,10] was constructed by stacking 10^3 such 1 ton detector modules, the detector would stretch around 1 km. Of course, the optimal segmentation of the detector depends on the application. Moreover, the distance between layers and the thickness of the layers may be adjusted depending on spacial constraints, required event rates, and desired angular resolution. A liquid scintillator may also be used instead of plastic scintillator.

Depending on the application and detector size, it may be beneficial to include charged-particle tracking, such as a wire chamber, between layers. Moreover, an ~ mT magnetic field can be incorporated to differentiate charged particles by the curvature of their tracks within the gap. This would help measure $\mathbf{p}_{e^+}$ and reduce backgrounds by requiring a positron in the final state; for example, radioisotope backgrounds typically result in a neutron and an electron, not a positron. With that said, a more realistic detector simulation should include cosmogenic, radiogenic, and fast neutron backgrounds. Depending on the application, directionality can be used to increase the signal-to-background ratio.

IBD may also occur in the capture layer, but most of these events are easily distinguished from the IBD events that originate in the target layer, because in the former scenario the positron first deposits energy in the capture layer. However, a finite energy threshold in the scintillator layers would introduce a source of background, where IBD occurs in the capture layer, but the positron escapes, depositing less energy than the threshold and then travels through the adjacent target layer. For typical energy thresholds ~200 keV and below and a target-layer thickness ~1 cm, this source of background is negligible, since a positron deposits ~ MeV of energy through ionization per centimeter in plastic. Charged-particle tracking between layers would eliminate this background completely. Another way of eliminating this background would be to use a neutron detector without hydrogen, such as a ^{3}He neutron detector. For these reasons, we do not include this background in our simulations, though its relevance should be assessed for specific detector designs.

It is also important to note that SANTAs may have directional sensitivity to ν_e-e^- and $\bar{\nu}_e$-e^- elastic scattering; we may reconstruct the momentum of the recoiling electron by tracking it through the detector. This makes our detector well suited, for example, for studying antineutrino-electron elastic scattering with an artificial antineutrino source, such as a nuclear reactor or IsoDAR [32]. Moreover, the elastic scattering events show up as double coincident signatures; the e^- deposits energy in both layers, with a few-nanosecond delay. With charged-particle tracking, the e^- may also be tracked and identified between layers. These extra pieces of information help reduce background as compared to the same processes in monolithic detectors.

A first-stage experiment might consist of a small detector placed near a nuclear reactor. For example, consider a SANTA with a single 2 cm thick 2×2 m^2 target layer, between two 6 cm thick equal-area capture layers placed ~25 m away from the core of a 3.4 GW$_{\text{th}}$ nuclear reactor, similar to the SONGS experiment [33]. Roughly 500 IBD events would occur per day within the target layer, and an additional $\sim 3 \times 10^3$ events would occur per day in the capture layers that could be used for nondirectional detection. Such an experiment may have applications to near-field nuclear reactor monitoring and searches for new physics in the neutrino sector, while also paving the way for larger detectors.

In a follow-up work, we will present a thorough detector simulation, including backgrounds and realistic detector properties, for a SANTA in the vicinity of a nuclear reactor.

The authors would like to thank F. Calaprice, J. Conrad, J. Formaggio, P. Huber, S. Lee, M. Lisanti, J. Spitz, M. Toups, C. Tully, and M. Vagins for helpful discussions. B. R. S. wishes to thank the Aspen Center for Physics supported in part by the U.S. NSF Grant No. PHYS-1066293, and Princeton University for hospitality during this work. B. R. S was supported in part by a Pappalardo Fellowship in Physics at MIT and in part by the U.S. Department of Energy under Grant No. DE-SC00012567. B. S. is supported by the U.S. Department of Energy under Grant No. ER-41850. The simulations presented in this article were performed on computational resources supported by the Princeton Institute for Computational Science and Engineering (PICSciE) and the Office of Information Technology's High Performance Computing Center and Visualization Laboratory at Princeton University.

*bsafdi@mit.edu
†suerfu@princeton.edu

[1] A. Bernstein *et al.*, arXiv:nucl-ex/0108001.
[2] M. M. Nieto *et al.*, arXiv:nucl-th/0309018.

[3] A. Bernstein, G. Baldwin, B. Boyer, M. Goodman, J. Learned, J. Lund, D. Reyna, and R. Svoboda, Science and global security: the technical basis for arms control and environmental policy initiatives **18**, 127 (2010).
[4] E. Christensen *et al.*, arXiv:1312.1959.
[5] E. Christensen, P. Huber, P. Jaffke, and T. E. Shea, Phys. Rev. Lett. **113**, 042503 (2014).
[6] C. Aberle *et al.*, arXiv:1307.2949.
[7] A. Bungau *et al.*, Phys. Rev. Lett. **109**, 141802 (2012).
[8] G. Fiorentini, M. Lissia, and F. Mantovani, Phys. Rep. **453**, 117 (2007).
[9] T. Araki *et al.*, Nature (London) **436**, 499 (2005).
[10] G. Bellini *et al.*, Phys. Lett. B **687**, 299 (2010).
[11] J. Schechter and J. W. F. Valle, Phys. Rev. D **24**, 1883 (1981).
[12] J. Schechter and J. W. F. Valle, Phys. Rev. D **25**, 283 (1982).
[13] B. Zel'dovich and O. Kh., Sov. Phys. Dokl. **10**, 524 (1965).
[14] M. A. Ruderman, Rep. Prog. Phys. **28**, 411 (1965).
[15] O. Kh., Sov. Astron. **10**, 613 (1967).
[16] J. F. Beacom, Annu. Rev. Nucl. Part. Sci. **60**, 439 (2010).
[17] G. Zacek *et al.*, Phys. Rev. D **34**, 2621 (1986).
[18] Y. Declais *et al.*, Nucl. Phys. **B434**, 503 (1995).
[19] F. Boehm *et al.*, Nucl. Phys. B, Proc. Suppl. **77**, 166 (1999).
[20] F. Boehm *et al.*, Phys. Rev. D **64**, 112001 (2001).
[21] M. Apollonio *et al.*, Eur. Phys. J. C **27**, 331 (2003).
[22] H. K. M. Tanaka and H. Watanabe, Sci. Rep. **4**, (2014).
[23] J. Learned, in Proceedings of Advances in Neutrino Technology, Philadelphia, 2011.
[24] J. V. Dawson and D. Kryn, JINST **9**, P07002 (2014).
[25] S. Agostinelli *et al.*, Nucl. Instrum. Methods Phys. Res., Sect. A **506**, 250 (2003).
[26] http://www.eljentechnology.com/index.php/products/loaded-scintillators/78-ej-254.
[27] Y. Kuroda, S. Oguri, Y. Kato, R. Nakata, Y. Inoue, C. Ito, and M. Minowa, Nucl. Instrum. Methods Phys. Res., Sect. A **690**, 41 (2012).
[28] Z. Djurcic *et al.*, arXiv:1309.7647.
[29] V. Belov *et al.*, JINST **8**, P05018 (2013).
[30] See the Supplemental Material at http://link.aps.org/supplemental/10.1103/PhysRevLett.114.071802 for further details of the analyses and additional detector simulation examples, which includes Refs. [26,31].
[31] P. Vogel and J. F. Beacom, Phys. Rev. D **60**, 053003 (1999).
[32] J. M. Conrad, M. H. Shaevitz, I. Shimizu, J. Spitz, M. Toups, and L. Winslow, Phys. Rev. D **89**, 072010 (2014).
[33] N. Bowden *et al.*, Nucl. Instrum. Methods Phys. Res., Sect. A **572**, 985 (2007).